Journal of Power Sources 242 (2013) 447–454

Contents lists available at SciVerse ScienceDirect

Journal of Power Sources

journal homepage: www.elsevier.com/locate/jpowsour

Dynamic electrochemical impedance spectroscopy of Pt/C-based membrane-electrode assemblies subjected to cycling protocols

Mahdi Darab [a], Per Kristian Dahlstrøm [a], Magnus Skinlo Thomassen [b], Frode Seland [a], Svein Sunde [a,*]

[a] Department of Material Science and Engineering, Norwegian University of Science and Technology NTNU, 7491 Trondheim, Norway
[b] SINTEF Materials and Chemistry, NO-7465 Trondheim, Norway

HIGHLIGHTS

- PEM fuel cell MEAs subjected to potential cycling were characterized in-situ by dynamic EIS.
- Moderate particle growth and agglomeration were observed during cycling.
- This led to significant changes in the impedance spectra.
- Thus changes in the catalyst structure lead to a change in the reaction mechanism.

GRAPHICAL ABSTRACT

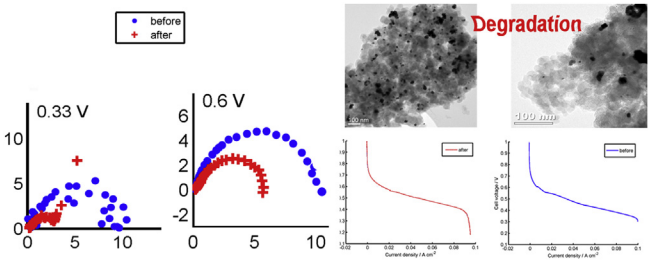

ARTICLE INFO

Article history:
Received 7 December 2012
Received in revised form
29 April 2013
Accepted 23 May 2013
Available online 5 June 2013

Keywords:
Electrocatalyst
PEMFC
Pt nanoparticles
dEIS
Activation

ABSTRACT

A PEM fuel cell membrane–electrode assembly (MEA) was characterized by dynamic electrochemical impedance spectroscopy (dEIS) before and after cycling in a single cell configuration. The cell was subjected to 100 cycles between 0.6 V and 1.5 V vs. RHE in N_2/5% H_2 and 80 °C and 100% RH. Initially, the impedance-plane plots contained first- and fourth-quadrant behavior, which is resulting from a reaction mechanism at the cathode involving adsorbed intermediates. After the cycling, the impedance spectra changed to display first-quadrant behavior only. This is suggested to be due to particle growth and possibly the formation of edges between agglomerated particles. The results show that dEIS is a sensitive technique to detect even very moderate changes in electrocatalyst structure.

1. Introduction

Although Proton Exchange Membrane Fuel Cells (PEMFCs) have come a long way to be an efficient source of power, there are still shortcomings to be addressed. This includes stability issues, for which there are stringent technical requirements to fulfill [1–4]. It is therefore important to quantify and understand activation and degradation of PEMFC components. In particular there is a need for an understanding and early-fault detection of degradation of electrode catalysts. The cathode appears especially prone to degradation due to its excursion to high potentials and repeated forming and removal of Pt oxide layers. Due to catalyst restructuring, place-exchange during this process [5] and subsequent loss of catalyst coordination, the cathode is therefore one of the major sources of performance loss in PEM fuel cells. On the other hand the oxygen reduction reaction at the cathode is highly sensitive to the electrode structure [6,7]. Therefore, surface restructuring due to degradation will be subject to mechanism changes and possibly

* Corresponding author. Tel.: +47 7359 4051; fax: +47 73591105.
E-mail addresses: svein.sunde@ntnu.no, Svein.Sunde@material.ntnu.no (S. Sunde).

0378-7753/$ – see front matter © 2013 Elsevier B.V. All rights reserved.
http://dx.doi.org/10.1016/j.jpowsour.2013.05.105

also activity changes. To understand these possible changes and in particular to detect them at an early stage, development of associated sensitive characterization and diagnostic techniques such as those suggested by others [8–11] are required.

Electrochemical impedance spectroscopy (EIS) is a robust diagnosis tool for studying fuel cells and fuel cell reactions, including those relevant for PEM fuel cells [12,13]. The simplest use of EIS is for estimation of the ohmic and charge transfer resistances [14–17], for which the technique is now routinely used. More sophisticated analysis of EIS data offers in addition information complementary to that obtained from polarization curves and cyclic voltammetry alone, such as information pertaining to electrode structure and electrode reaction mechanisms. As such, EIS offers a resolution not available in polarization curves since the different processes that contribute to the acquired data can be separated in frequency [12,18].

There are a few examples showing that the shape of the impedance spectrum alone can give clear indications of a certain reaction mechanism out of the subset of mechanisms possible under the prevailing reaction conditions [19,20]. A prominent example of the use of EIS in diagnosis of electrochemical systems in terms of reaction mechanism is the study of processes involving multi-step reactions with adsorbed intermediates [20,21]. Thus, a low-frequency inductive loop that appears in the impedance spectra of point contacts of Pt and Ni at YSZ in CO and CO_2 is only consistent with at least two adsorbed intermediates taking part in the reaction [22,23]. Another relevant example is the study performed by Müller and co-workers on a direct methanol fuel cell anode [24,25]. They showed that an inductive loop appears under pure kinetic control, while two capacitive loops are present when introducing significant mass-transfer limitations [24].

Usually, EIS is performed under steady-state conditions. In dynamic impedance spectroscopy (dEIS) [26], on the other hand, EIS spectra can be collected also for systems under dynamic conditions. Thus, a multi-sine wave consisting of all frequencies of interest is superimposed on a dc potential ramp. This provides the possibility to collect kinetic information on transient surfaces, which is not available in electrochemical impedance spectroscopy under steady-state conditions. This may be important for example if one wants to detect the presence of (short-lived) adsorbed intermediates in electrochemical reactions. Also polarization curves can be extracted from the measurements simultaneously with the impedance spectra. This enables direct correlation between the impedance spectra and features in the fuel cell performance in this case. Since all frequencies are applied simultaneously in the dEIS technique, a fast Fourier transform (FFT) algorithm is used to separate each frequency's current response. dEIS is also different from ac voltammetry, since in the latter technique impedance spectra are collected one frequency per potential scan. As a consequence there will be a time lapse between the first and the last measured frequency which may be the source for some drift effects [27,28]. Such time effects are eliminated with the dEIS technique.

There is also solid evidence of the feasibility for studying the activation and degradation processes on electrodes and membranes in fuel cells by EIS [29,30]. Although EIS has been applied to some extent for studying the aging of electrodes by EIS at constant current or potential [31–34], less attention has been paid to impedance spectroscopy at electrocatalysts undergoing potential cycling. Also, ex-situ measurements [12,29] appear to dominate over in-situ techniques [35,36]. To the best of our knowledge there is but very limited data dealing with establishment of a link between overall electrocatalyst activation and degradation and its impedance spectra evolution in-situ. As far as the application of EIS in PEM fuel cell diagnostics are concerned there appears to be at least two possibilities for improvement: i) applications of EIS with comprehensive studies on MEAs in-situ, and ii) investigations on degradation phenomena using a potential cycling protocol, which is different than an aging protocol at a constant current density or potential. A combined perspective is to have an in-situ detectable EIS response to the changes in reaction mechanism occurring as a consequence of a wide-range potential cycling degradation.

In the present study we pursue the mitigation of these two shortcomings by presenting an approach to study the properties of a cycled MEA based on dynamic electrochemical impedance spectroscopy. The appearance of a resolved semicircle and an inductive loop for the pristine sample and an additional partially developed semicircle for the cycled MEA will be discussed in the light of a plausible mechanism change under the cycling protocol.

2. Experimental

The experimental part in this work includes the synthesis of the Pt/C electrocatalyst and corresponding physical and structural characterization and microscopy and ex-situ electrochemical characterization in the first step and then fabrication of MEAs and relevant in-situ electrochemical measurements in the second step. The following provides a detailed explanation of each sub-step.

2.1. Synthesis of electrocatalyst

The polyol technique was used to synthesize the electrocatalysts as described in detail elsewhere [37]. In brief, the support material (carbon black) was dispersed in ethylene glycol (EG) and kept at 50 °C for 30 min. Platinic acid, already dissolved in ethylene glycol, was added to the mixture and the temperature was increased to 110 °C under a nitrogen flow. The mixture was kept at elevated temperature for 1.5 h followed by cooling step in the air and centrifuging the catalyst, ultrasonic homogenization, and washing with water and acetone. The sample was dried at 80 °C for 8 h.

The sample used in this study comprised 15 wt% platinum on Vulcan XC-72 carbon support and accordingly marked as XC15. The actual metal loading was estimated from the residue of the TGA experiment in oxygen atmosphere from room temperature to 800 °C with a heating rate of 10 °C min^{-1} using an NETZCH system model STA 449C.

2.2. Transmission electron microscopy

A JEOL JEM-2010 transmission electron microscope was used to estimate the particle size and assess the metal distribution on the support both before and after the cycling. TEM was performed on the pristine sample as synthesized and on the extracted catalyst from the MEA, which was carefully scraped away from the cathode side of the cycled MEA.

2.3. Electrochemical studies in liquid cell

The electrochemical measurements were carried out in a 0.5 M $HClO_4$ solution in a conventional three-electrode cell at room temperature. Ar was bubbled for 30 min prior to the experiment to remove any dissolved oxygen from the electrolyte. The electrolyte was kept under an Ar blanket during the course of the experiment.

A reversible hydrogen electrode (RHE) was used as reference electrode and a 1.5 cm^2 plate of pure platinum as counter electrode. An electrocatalyst ink was prepared by sonication of 1.0 mg of the catalyst in 1.0 mL of water. Then 20.0 μL of the ink was pipetted on a disk-type glassy carbon (GC) and dried in N_2, followed by addition of 20 μL Nafion® to cover the working electrode. The area of the GC electrode was 0.196 cm^2. The CVs and CO stripping experiments were performed with an Autolab potentiostat model PGSTAT302N

along with a three-electrode cell equipped with necessary connections for Ar and CO. The CO electro-oxidation protocol applied in this study was to run cyclic voltammetry (CVs) 20 times at the rate of 100 mV s^{-1} followed by 5 CVs at 10 mV s^{-1}. CO was admitted to the electrode at a potential of 20 mV vs. RHE [38]. Dissolved CO was removed from the cell by an argon purge. In these experiments the CO electro-oxidation normally occurred at 10 mV s^{-1}. The experiment was finalized by performing four CVs at 10 mV s^{-1}.

2.4. Membrane electrode assembly

In order to prepare an MEA, a Nafion® 115 membrane (DuPont) was cleaned by boiling, first in 3% aqueous H_2O_2 solution for 1 h, followed by 1 h boiling in 0.5 M H_2SO_4, and eventually boiled in Milli-Q water for 15 min. The membrane was finally dried in an oven at 70 °C for 15 min. The ink of the catalyst was prepared by mixing the Pt/C electrocatalyst powder with the nominal targeted metal mass loading together with 5 wt% Nafion® solution (DuPont), using Milli-Q (18.2 MΩ) distilled water and isopropanol all in analytical grades, in equal volumetric amounts as solvent.

The ink was homogenized in an ultrasound bath and magnetically stirred for a short period before spraying by airbrush (Badger 360 G) on the membrane. The membrane was located on a hot plate at 90 °C for evaporation of the solvents and a more homogenous coating. The area of the resulting electrode was 5 cm^2 and had the loading of 0.4 mg_{Pt} cm^{-2}. A commercial gas diffusion electrode (GDE) from ETEK consisting of 20 wt% Pt/Vulcan XC-72 with 0.5 mg_{Pt} cm^{-2} loading on a gas diffusion layer (GDL) was employed for the anode side while the synthesized catalysts served on the cathode side along with commercial SIGRACET gas diffusion media, GDL 35BC. The catalyst-coated Nafion® was hot pressed with the anode GDE at 130 °C and 1400 kPa for 1 min and the GDL was then mounted on the cathode side to form the MEA.

2.5. Fuel cell configuration and in-situ electrochemical studies

A standard commercial PEM fuel cell hardware was used in this study where the MEA was placed inside the cell. The gas inlets were connected to gas humidifiers to reach 100% RH for the incoming gases while the junctions were well sealed to avoid any condensation and unwanted temperature gradients.

Humidified hydrogen and oxygen (5.0) were fed into the anode and cathode, respectively. With the intention of avoiding issues related to gas cross-over, pure hydrogen was replaced by harmix (5% H_2 balanced with Ar) during the cycling test. Oxygen was also substituted with nitrogen for the voltammetric cycles included in the protocol. The gas flow rate for the anode and cathode inlets was minimum 0.10 l_n min^{-1} and 0.22 l_n min^{-1} respectively to avoid any gas starvation. The fuel cell characteristics were drawn using an Agilent N3300A system. The cell was operated at 80 °C. To avoid gas condensation in the system, the pipe temperature was set to 82 °C.

In-situ cyclic voltammetry and the cycling protocol were conducted by a Biologic SP-150 potentiostat with a 2A booster. The incoming gases were N_2 on the cathode side and harmix on the anode side. The experiment was carried out at 100% RH and room temperature. In-situ CO stripping was also carried out with the same potentiostat and booster configuration and gas inlet except for a replacement of 100 ppm CO in H_2 with the harmix to facilitate CO adsorption.

The fuel cell was characterized with dynamic electrochemical impedance spectroscopy (dEIS). In this experiment a Keithley KUSB-3116 module was used for generation of the multi-sine wave and data logging, a Princeton Applied Research Model 175 waveform generator was used to create the dc potential scan, and the AC and DC components of the potential wave were summed together with Stanford Research System (SRS) Small Instrumentation Modules (SIM). A Gamry Reference 600 potentiostat in analog mode was used to apply the potential signal to the fuel cell. During the dEIS measurements, the time, ac and dc components of the cell potential, and the total cell current were recorded. After the experiment, a custom-made software invokes an FFT algorithm to calculate the impedance at all potentials scanned over according to Ref. [26]. In our experiments 46 frequencies in the range 0.2 Hz–2.6 kHz were superimposed on a slow (1 mV s^{-1}) DC potential scan. A sketch of the dEIS setup is presented in Fig. 1.

In this study the whole set of in-situ electrochemical measurements were repeated after a cycling protocol of 100 CVs between 0.6 V and 1.5 V vs. RHE in N_2/5% H_2 and 80 °C and 100% RH using a sweep rate of 40 mV s^{-1}. O_2 and H_2 flow rates were 24.8 mL s^{-1} and 80 mL^{-1} respectively.

3. Results and discussion

Transmission electron micrographs for pristine XC15 are shown in Fig. 2 on a range of scales from micron to nanometers. It is apparent that the electrocatalyst consist of both individual and aggregated Pt nanoparticles.

Fig. 3 shows high-resolution TEM images of catalyst scraped away from an MEA surface after it was subjected to the cycling protocol. The images show the same spot of the sample at increasing magnification, the order of which are indicated by the red arrows, in web version. The catalyst particles in the cycled sample in Fig. 3 appears to be more aggregated than those in the pristine sample, indicating some particle growth during the potential cycling.

Fig. 4 shows the collective histograms of platinum particle size from a number of TEM images of pristine and cycled samples. From the histograms there are clear signs of particle growth, and the shape of the distribution for the cycled sample is skewed toward larger diameters relative to that of the pristine samples. The mean particle size for fresh sample is 18.3 ± 0.4 nm while for the MEA of XC15 it is 21.8 ± 0.5 nm.

The particle growth is thus rather moderate. However, quite large particles are present in the fresh sample. These already aggregated Pt particles would not be expected to show a significant tendency for further aggregation. The average increase in diameter may therefore underestimate slightly the actual growth in the most active part of the catalyst, viz. the smaller particles. In summary, a small but detectable growth in particle size is present as a consequence of the cycling protocol.

An ex-situ CO stripping voltammogram of the pristine catalyst is shown in Fig. 5. CO oxidation appears as a double oxidation peak. The larger of these appears at approximately 0.79 V, which is a characteristic value for individual Pt particles. The smaller peak appears at approximately 0.72 V. CO electro-oxidation may occur at multiple potentials in samples with aggregated particles [6,39]. In view of the agglomeration apparent in the TEM images in Fig. 2, we therefore interpret the double peak as being a consequence of particle agglomeration. The peak at 0.72 V may thus corresponds to grain boundaries or other defects associated with the agglomeration.

The electrochemically active surface area (ESA) in the pristine catalyst was estimated to 15.83 m^2 g^{-1} based on the charge transferred during the CO electro-oxidation assuming CO monolayer bonded with one Pt atom in a linear adsorption configuration (Pt–CO_{ads}), and the equation [40]:

$$\mathrm{ESA_{CO}}\left(\mathrm{m^2\,g^{-1}}\right) = \left(Q_{\mathrm{CO}}(\mathrm{C})/420\left(\mathrm{mC\,cm^{-2}}\right)\right)\cdot W_{\mathrm{Pt}}(\mathrm{g})\cdot 100 \quad (1)$$

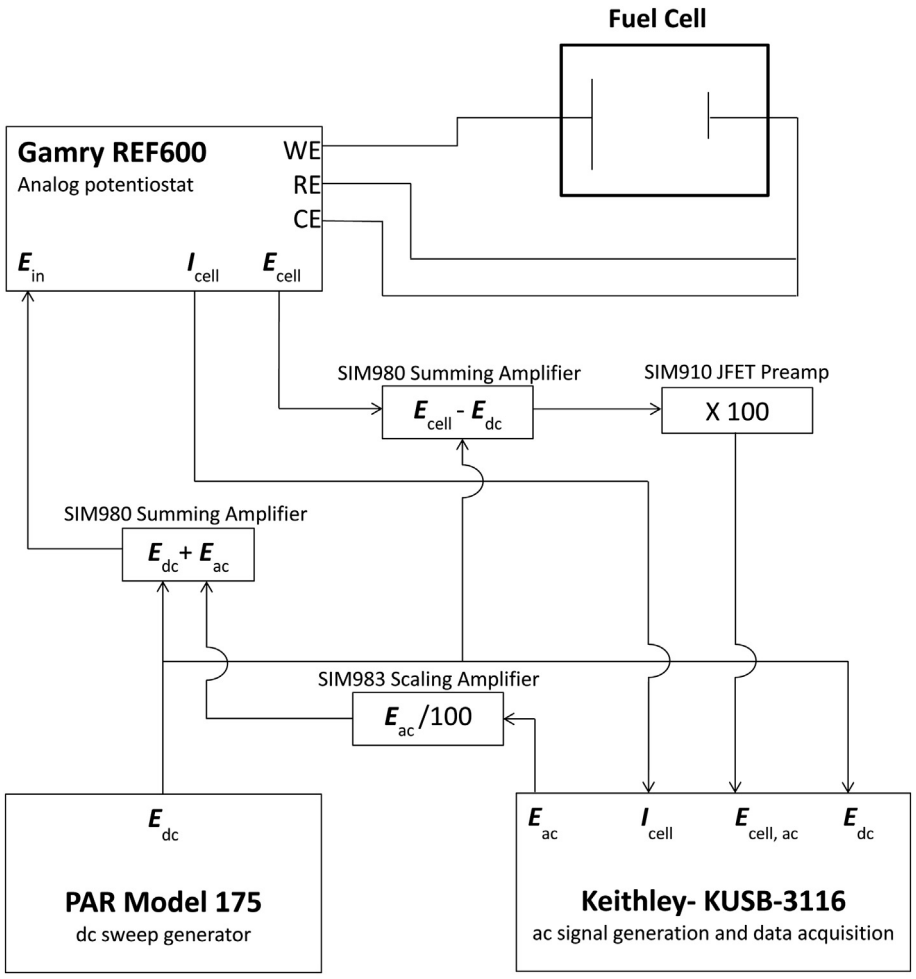

Fig. 1. Sketch of the dEIS setup.

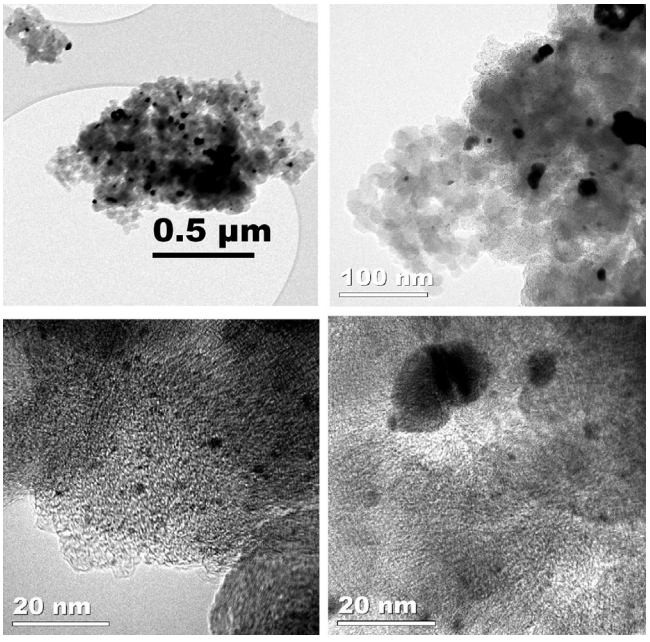

Fig. 2. TEM micrograph from the pristine 15% Pt/XC-72 (XC15) sample powder.

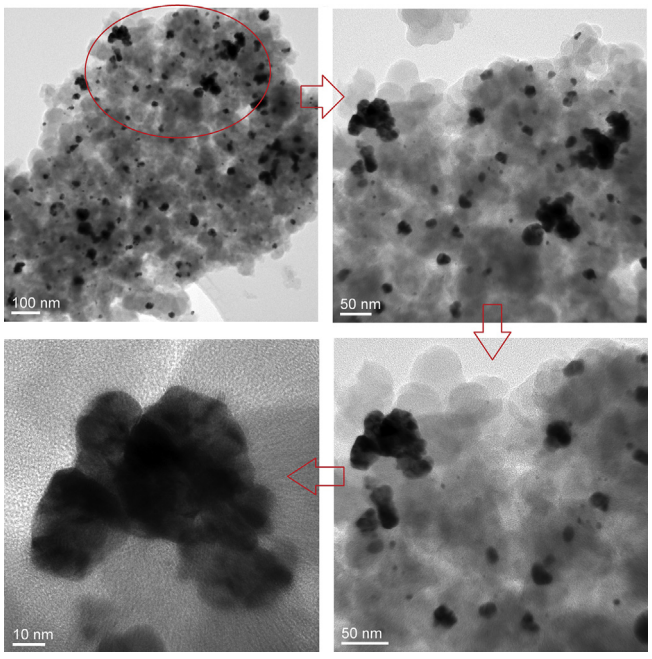

Fig. 3. TEM images of powder scraped away from the cathode surface of the cycled MEA of XC15.

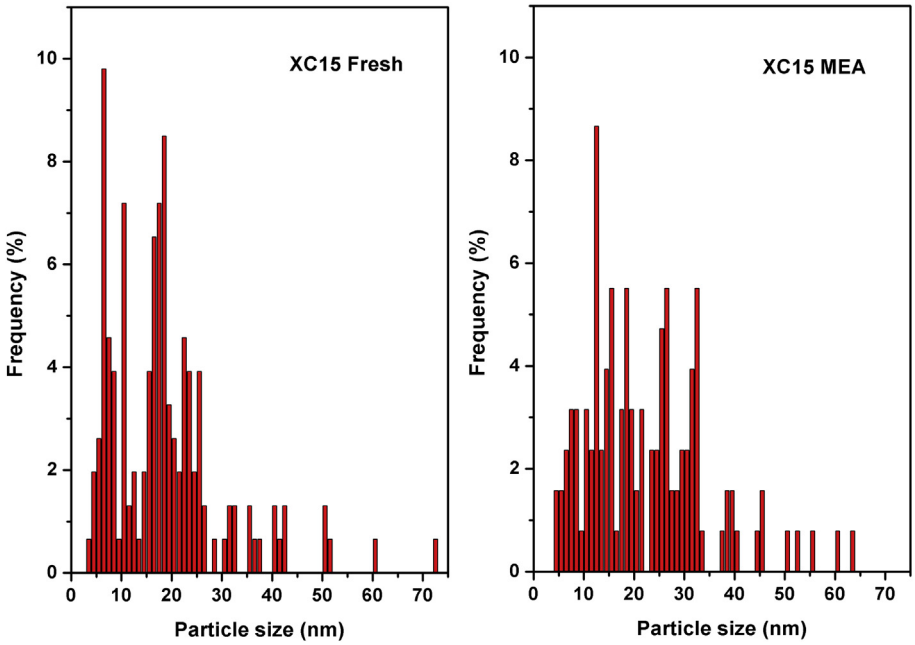

Fig. 4. Histograms of platinum nanoparticles in Figs. 2 and 3 for pristine and cycled samples.

where Q_{CO} is the charge transferred related to CO oxidation reaction, 420 mC cm^{-2} is the charge required to oxidize CO monolayer bonded with one Pt atom in a linear adsorption configuration and W is Pt loading.

In-situ CO stripping voltammograms recorded on XC15 before and after the cycling protocol are shown in Fig. 6. In the fresh sample there is no peak splitting apparent as in the ex-situ stripping voltammogram (Fig. 5). Apparently, the in-situ CO-stripping is less sensitive to agglomeration than ex-situ stripping. We relate this fact to the difference in catalyst mass and the thickness in the two cases. In a porous layer, as in the in-situ experiment, the current and potential are distributed through the layer. Similar changes in the hydrogen-adsorption region are also frequently observed [41,42]. However, in view of the shoulder at 0.76 V in the cycled sample, it does appear possible to also use CO stripping voltammetry in-situ to assess agglomeration in the catalytic layer. In the stripping voltammogram of the cycled sample a small shoulder has developed, again indicating moderate agglomeration as a consequence of the cycling protocol.

The ESA was estimated in the same range as the data extracted from the ex-situ CO stripping voltammetry and showed a loss of around 17%. Table 1 summarizes the mean particle size and ESA for the pristine and cycled electrocatalysts.

In-situ CVs of the fresh and cycled samples shown in Fig. 7 demonstrate a very slight alteration in the H_2 adsorption/desorption area indicating a minor change in electrochemical surface area for Pt particles as discussed earlier. The CVs in Fig. 8 comply with the indications in TEM pictures and corresponding histograms of particle size distribution that the Pt particles were only moderately affected by the accelerated cycling.

Impedance spectra obtained with dEIS measurements at selected cell voltages before and after the cycling procedure are shown in Fig. 8. At high cell voltages (low overpotentials), the impedance is large and forms an incipient semicircle in the first

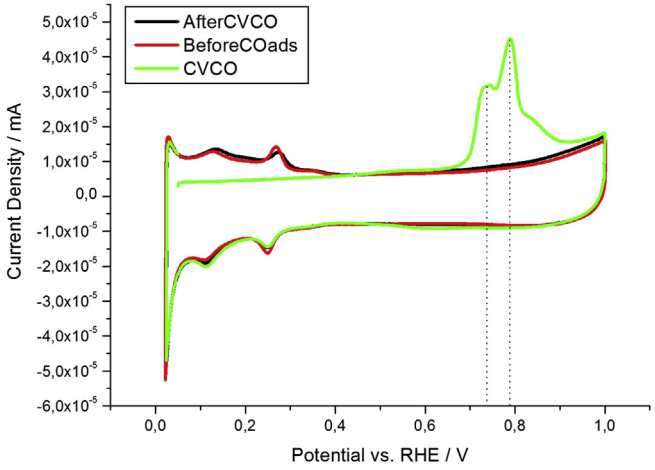

Fig. 5. CO stripping voltammograms at a sweep rate of 10 mV s^{-1} for XC15. The electrolyte was 0.5 M $HClO_4$ and Ar was maintained inside the cell during the experiment at room temperature.

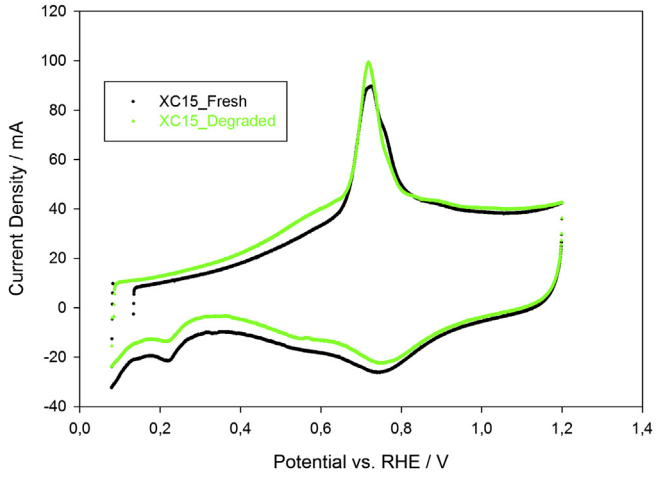

Fig. 6. In-situ CO stripping voltammetry for the sample XC15 before and after the cycling. Gases: N_2/harmix for CVs (100 mV s^{-1}) and CO/harmix for CO adsorption (150 mV vs. RHE). The experiment was carried out at 100% RH and room temperature.

Table 1
Properties of the sample XC15, 15% Pt/XC-72, synthesized by polyol before and after the cycling protocol.

Property↓	Value→		
	Pristine sample	Cycled sample	Change upon cycling
Mean particle size[a] (nm)	18.3 ± 0.4	21.8 ± 0.5	+17%
ESA[b] ($m^2\ g_{Pt}^{-1}$)	15.8	13.2	−16%

[a] Obtained from histograms of particle size distribution from TEM images shown in Fig. 4.
[b] Obtained from ex-situ CVs (for the pristine sample) and in-situ CVs (for the cycled sample).

quadrant. As the voltage decreases, the low-frequency limit of the total impedance decreases as expected since the overpotential increases. The shape then develops into a full semicircle. The radius of the impedance spectra is lower after cycling than for the impedance before cycling, suggesting that the charge-transfer reactions have become faster. A similar behavior was also observed by Hu et al. [34].

At approximately 0.57 V, a loop in the fourth quadrant appears in the low-frequency part of the impedance spectra obtained before cycling (The low frequency part of the spectrum bends back toward the origin of the impedance plan and simultaneously the imaginary part becomes positive.). This inductive loop is often associated with an adsorbed species. After cycling, on the other hand, the inductive loop is not present anymore, except that may be one or two points in the data collected at 0.54 and 0.51 V can be interpreted as an incipient inductive feature of the plot. However, for all the others, all data remain in the first quadrant, and do not curve back toward the origin. Instead, another, first-quadrant semicircle appears below 0.45 V. As the cell voltage is decreased further, this semicircle becomes more visible in the impedance-plane plots.

Quasi-steady-state polarization curves obtained simultaneously as the impedance spectra shown in Fig. 8 are shown in Fig. 9. These polarization curves show the effect of the cycling protocol. Between 0.75 V and 0.35 V, the current is slightly higher after the cycling. The limiting current is shifted to lower values after the cycling (Due to current limitations in the set-up, the polarization curve had to be stopped at approximately 0.3 V before cycling and at approximately 0.2 V after.).

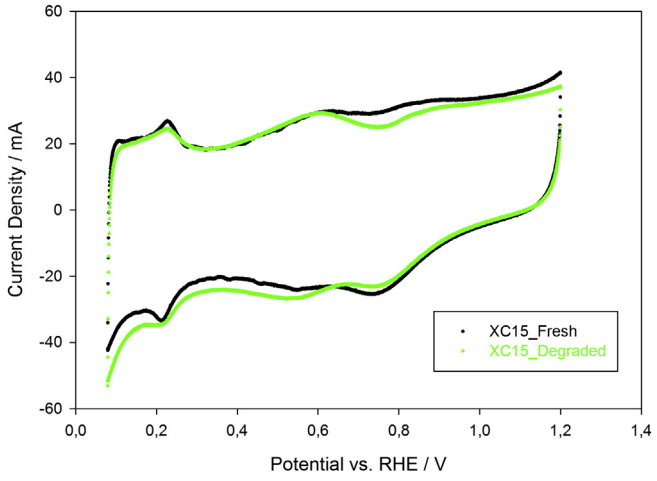

Fig. 7. In-situ anodic cyclic voltammograms for the sample XC15 before and after the cycling. Gases were N_2 on anode side and harmix on cathode side. Sweep rate was 100 mV s^{-1}. The experiment was carried out at 100% RH and room temperature.

Our findings thus indicate that the moderate agglomeration introduced in the samples by the potential cycling leads to an improved activity for CO-stripping as reported before and also for the oxygen-reduction reaction (ORR). The latter is in line with the results of Hu et al. [34], who reported impedance spectra showing the effect of time for a fuel cell maintained at constant current for 500 h. The charge-transfer resistance was found to decrease to a minimum for the first 100 h, and then increase for the remainder of the experiment. They termed the former phase the activation phase, and the latter phase the degradation phase.

Although the polarization curves in Fig. 9 only display a limited effect of the cycling procedure, the impedance spectra in Fig. 8 prove otherwise, since a significant change is seen. This suggests that EIS is a technique that is sensitive enough to study the effects of cycling on fuel cell systems.

The appearance of incipient, second semicircle in the impedance diagrams in Fig. 8 appears to correlate with the potential at which the limiting current appear in Fig. 9. When the potential reaches approximately 0.4 V the first few points tracing out a second feature (semicircle) appear in the in the impedance plane plot (compare impedance plane plots collected at 0.45 V and 0.42 V). It is not easy to define the exact shape of this part of the curve. However, the fact that it appears to bend over rather than rising indefinitely is qualitatively consistent with finite-length diffusion [43], or with simultaneous reaction and diffusion (Gerischer element, see e.g. Ref. [22]). We therefore tentatively associate this feature of the spectra with transport limitations in the MEA. However, since no Warburg-type sections appear in the plots, a definitive analysis of this feature will not be attempted here.

The inductive loop in the impedance plane plots in Fig. 8 for the pristine catalyst can in principle also be related to transport phenomena in the electrode, in addition to being related to the electrode kinetics as indicated in the Introduction. Impedance modeling based on flooded agglomerate theory shows that impedance spectra may contain inductive loops purely related to transport in the MEA [44]. However, this only applies if there are two mobile species in the electrolyte, which is not the case here. In the case where one electrolyte species in the model was immobilized, the inductive loop disappeared. In the following we therefore disregard structural changes in the MEA and associated changes in the transport properties as a cause for the changes in the impedance spectra as a result of potential cycling above 0.45 V.

During cycling, the structure of catalyst particles electrodes may change in various ways: Roughening, agglomeration, and dissolution. An explanation for the activation phase while the electrode undergoes a cycling protocol was offered by Nagy, who proposed that surface roughening induced by the oxidation/reduction of Pt atoms would lead to a location exchange with oxygen atoms [5,45]. This is, however, not consistent with the decrease in the EAS observed here, and we disregard the effect of roughening. An increase in particle size is, on the other hand, consistent with the decrease in the ESA, with the increased particle size in the TEM images, and also with the increased activity. Mayrhofer et al. [46] demonstrated a significant increase in the activity for the ORR with increasing particle size, interpreted in terms of changes in the work function with size. Kinoshita [47] has suggested that crystal facets are active for the ORR, whereas corners and edges are not. The reaction thus appears to be only moderately dependent on the concentration of steps in stepped Pt surfaces [48]. Therefore, this also implies that larger particles are more active.

Although the improved performance itself can be explained as due to growing particles, it is difficult to rationalize the initial presence and disappearance of the inductive loop upon cycling any other way than by a change in the reaction mechanism. The inductive loop indicates the involvement of two adsorbed

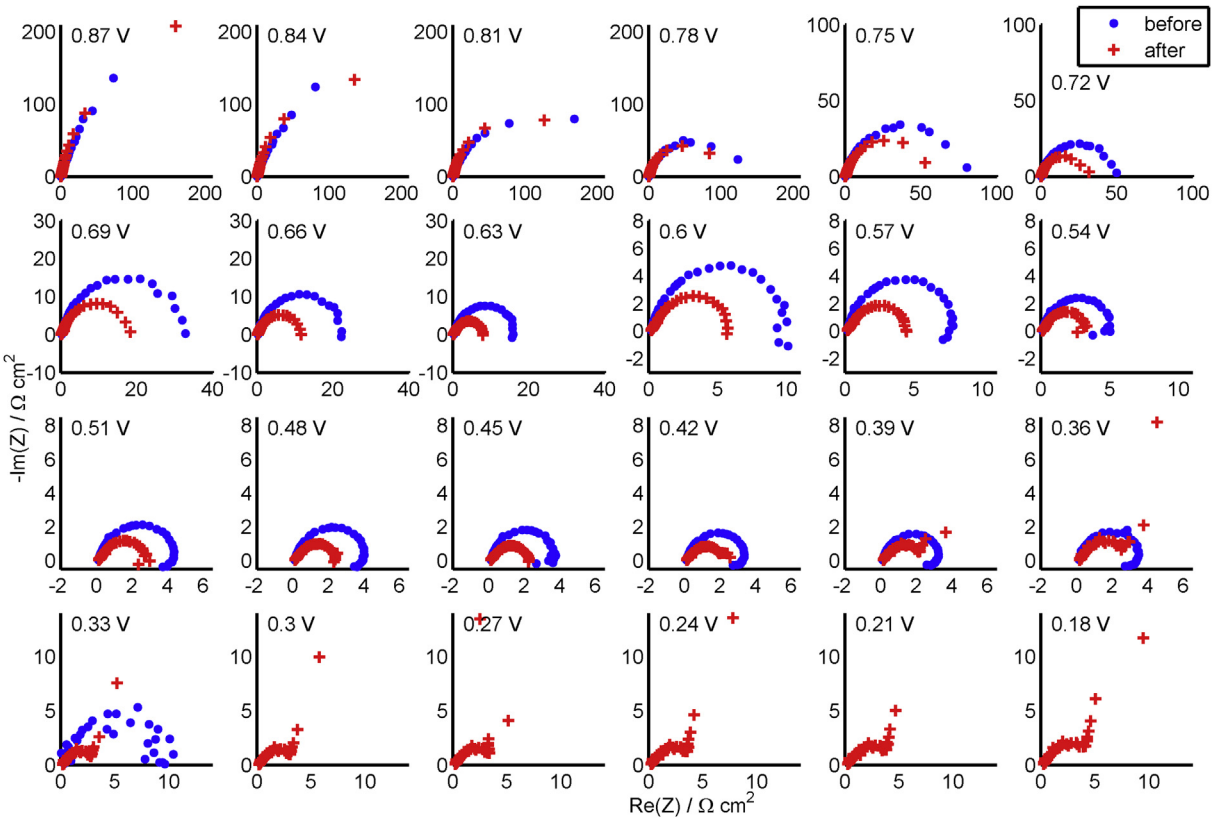

Fig. 8. Impedance spectra at selected cell voltages during the slow potential scan for XC15 MEA before and after the cycling.

intermediates taking part in the rate-determining step of the reaction. This would be compatible with a large number of reaction mechanisms proposed for the ORR, e.g. involving hydrogen peroxide path for which the rate-determining step is the reaction between two different adsorbates on the Pt surface under acidic conditions [49] (A reaction including the formation of hydrogen peroxide as an intermediate step in a two-step reaction was recently shown to give inductive loops in impedance plane plots [50].). It is difficult to explain this with particle growth alone. Lopéz-Cudero et al. [51] recently suggested that the improved activity of agglomerated Pt catalysts is due to the formation of edges at the interface between two different nanoparticles in contact (thus being agglomerated). These edges and an adjacent crystal plane may form a locally concave surface, and are different from edges at single particles which would be convex. This may change the interaction between adsorbates at the edge and those at the adjacent crystal plane. Although the degree to which the ORR in general is structure-sensitive is still open [6], we suggest here that an effect similar to that proposed by Lopéz-Cudero in Ref. [51] is operative in the ORR and that the changes in the impedance spectra are related to edges between nanoparticles. Also, edges formed in the larger crystal facets of larger particles may give rise to a similar activity increase [6].

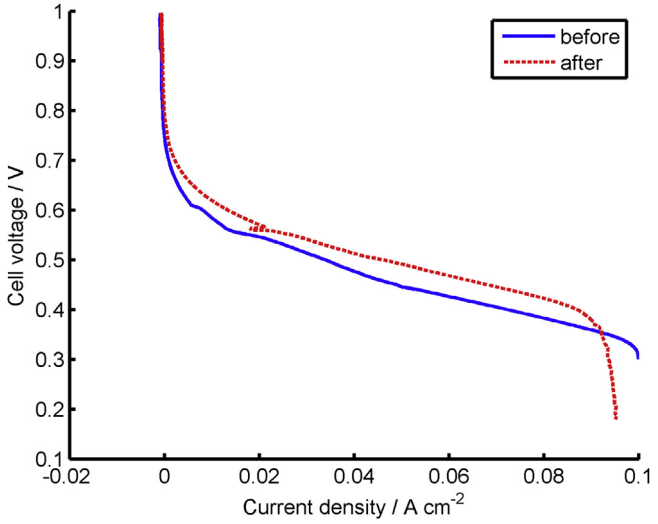

Fig. 9. Polarization curves obtained simultaneously as the impedance spectra when scanning the cell voltage at 1 mV s^{-1}.

Thus, the catalyst may become more active due to either larger particles or due to the formation of steps in the crystal facets or at interfaces between agglomerated particles. Our dynamic impedance data appears to indicate that this activity change is associated with a change in the reaction mechanism.

4. Conclusions

The polyol synthesized carbon supported Pt nanoparticles were characterized electrochemically ex-situ (in liquid electrolyte cell) and in-situ (in a single PEMFC) before and after a severe cycling protocol. The slight change in the structure of the electrocatalyst due to the cycling was not easy to detect by the other applied physical and electrochemical techniques than the dEIS method used here.

dEIS proved to be a convenient and time-efficient tool to gather impedance spectra for all cell voltages and to be a strong investigative tool to detect small modifications in electrodes which were not practically detectable by CVs, CO stripping, and TEM. With dEIS

we detected that the cycling protocol caused a change in the fuel cell reaction mechanism. These changes are suggested to be due to the formation of particularly active sites at growing crystal facets or at the interface between agglomerated particles.

Acknowledgment

Per Erik Vullum and Yingda Yu are thanked for the assistance with TEM imaging.

The financial support of the work by the Norwegian Research Council and the Department of Materials Science and Engineering, NTNU, is acknowledged.

References

[1] W. Vielstich, A. Lamm, H.A. Gasteiger, Handbook of Fuel Cells: Fundamentals, Technology, and Applications, Volume 2: Fuel Cell Electrocatalysis, Wiley, 2003.
[2] J. Healy, C. Hayden, T. Xie, K. Olson, R. Waldo, M. Brundage, H. Gasteiger, J. Abbott, Fuel Cells 5 (2005) 302–308.
[3] V. Mehta, J.S. Cooper, J. Power Sources 114 (2003) 32–53.
[4] J. Zhang, G.J. Offer, Platin. Met. Rev. 53 (2009) 219–220.
[5] Z. Nagy, H. You, Electrochim. Acta 47 (2002) 3037.
[6] M.T.M. Koper, Nanoscale 3 (2011) 2054–2073.
[7] B.J. Greeley, J. Rossmeisl, A. Hellman, J.K. Nørskov, Z. Phys. Chem. 221 (2007) 1209–1220.
[8] R.A. Silva, T. Hashimoto, G.E. Thompson, C.M. Rangel, Int. J. Hydrogen Energy 37 (2012) 7299–7308.
[9] J.H. Kim, Y. Yeon Jo, E.A. Cho, J.H. Jang, H.J. Kim, T.-H. Lim, I.-H. Oh, J.J. Ko, I.J. Son, J. Electrochem. Soc. 157 (2010) B633–B642.
[10] H. Chizawa, Y. Ogami, H. Naka, A. Matsunaga, N. Aoki, T. Aoki, ECS Trans. 3 (2006) 645–655.
[11] H.L. Lin, Y.S. Hsieh, C.W. Chiu, T.L. Yu, L.C. Chen, J. Power Sources 193 (2009) 170–174.
[12] X. Yuan, H. Wang, J. Colinsun, J. Zhang, Int. J. Hydrogen Energy 32 (2007) 4365–4380.
[13] S. Asghari, A. Mokmeli, M. Samavati, Int. J. Hydrogen Energy 35 (2010) 9283–9290.
[14] S. Zhang, X.-Z. Yuan, J.N.C. Hin, H. Wang, K.A. Friedrich, M. Schulze, J. Power Sources 194 (2009) 588–600.
[15] A.S. Arico', A. Stassi, E. Modica, R. Ornelas, I. Gatto, E. Passalacqua, V. Antonucci, ECS Trans. 3 (2006) 765–774.
[16] J. Xie, D.L. Wood, D.M. Wayne, T.A. Zawodzinski, P. Atanassov, R.L. Borup, J. Electrochem. Soc. 152 (2005) A104.
[17] M. Ciureanu, S.D. Mikhailenko, S. Kaliaguine, Catal. Today 82 (2003) 195–206.
[18] Y. Tang, J. Zhang, C. Song, H. Liu, J. Zhang, H. Wang, S. Mackinnon, T. Peckham, J. Li, S. McDermid, P. Kozak, J. Electrochem. Soc. 153 (2006) A2036–A2043.
[19] X. Yuan, C. Song, H. Wang, J. Zhang, Electrochemical Impedance Spectroscopy in PEM Fuel Cells, Springer, 2011.
[20] M.E. Orazem, B. Tribollet, Electrochemical Impedance Spectroscopy, John Wiley and Sons, New Jersey, 2008.
[21] J.R. Macdonald (Ed.), Impedance Spectroscopy: Emphasizing Solid Materials and Systems, John Wiley and Sons, New York, 1987.
[22] G.Ø. Lauvstad, R. Tunold, S. Sunde, J. Electrochem. Soc. 149 (2002) E497–E505.
[23] G.Ø. Lauvstad, R. Tunold, S. Sunde, J. Electrochem. Soc. 149 (2002) E506–E514.
[24] J.T. Müller, P.M. Urban, W.F. Hölderich, J. Power Sources 84 (1999) 157–160.
[25] J.T. Müller, P.M. Urban, J. Power Sources 75 (1998) 139–143.
[26] R.L. Sacci, D.A. Harrington, ECS Trans. 19 (2009) 31–42.
[27] F. Seland, R. Tunold, D.A. Harrington, Electrochim. Acta (2006) 3827–3840.
[28] R.E. Melnick, G.T.R. Palmore, J. Phys. Chem. B 105 (2001) 9449–9457.
[29] F.S. Saleh, E.B. Easton, J. Electrochem. Soc. 159 (2012) B546–B553.
[30] J. Kang, J. Kim, Int. J. Hydrogen Energy 35 (2010) 13125–13130.
[31] R. Lin, B. Li, Y.P. Hou, J.M. Ma, Int. J. Hydrogen Energy 34 (2009) 2369–2376.
[32] R. Escudero-Cid, P. Hernández-Fernández, J.C. Pérez-Flores, S. Rojas, S. Garcia-Rodríguez, E. Fatás, P. Ocón, Int. J. Hydrogen Energy 37 (2012) 7119–7130.
[33] M.K. Jeon, J.Y. Won, K.S. Oh, K.R. Lee, S.I. Woo, Electrochim. Acta 53 (2007) 447.
[34] J. Hu, H. Zhang, Y. Zhai, G. Liu, B. Yi, Int. J. Hydrogen Energy 31 (2006) 1855–1862.
[35] A. Marcu, G. Toth, S. Kundu, L.C. Colmenares, R.J. Behm, J. Power Sources 215 (2012) 266–273.
[36] Z. Lu, S.G. Kandlikar, C. Rath, M. Grimm, W. Domigan, A.D. White, M. Hardbarger, J.P. Owejan, T.A. Trabold, Int. J. Hydrogen Energy 34 (2009) 3445–3456.
[37] M. Darab, M. Thomassen, S. Sunde, ECS Trans. 41 (2011) 1067–1078.
[38] P. Ochal, J.L. Gomez de la Fuente, M. Tsypkin, F. Seland, S. Sunde, N. Muthuswamy, M. Rønning, D. Chen, S. Garcia, S. Alayoglu, B. Eichhorn, J. Electroanal. Chem. 655 (2011) 140–146.
[39] F. Maillard, S. Schreier, M. Hanzlik, E.R. Savinova, S. Weinkauf, U. Stimming, Phys. Chem. Chem. Phys. 7 (2005) 385–393.
[40] B.M. Rush, J.A. Reimer, E.J. Cairns, J. Electrochem. Soc. 148 (2001) A137–A148.
[41] R.W. Lindström, K. Kortsdottir, M. Wesselmark, A. Oyarce, C. Lagergren, G. Lindbergh, J. Electrochem. Soc. 157 (2010) B1795–B1801.
[42] H.N. Dinh, X. Ren, F.H. Garzon, S. Gottesfeld, J. Electroanal. Chem. 491 (2000) 222–233.
[43] E. Barsoukov, J.R. Macdonald, Impedance Spectroscopy: Theory, Experiment, and Applications, Wiley-Interscience, Hoboken, New Jersey, 2005.
[44] A.M. Svensson, H. Weydahl, S. Sunde, Electrochim. Acta 53 (2008) 7483–7490.
[45] Z. Nagy, H. You, Phys. B 198 (1994) 187–194.
[46] K.J.J. Mayrhofer, B.B. Blizanac, M. Arenz, V.R. Stamenkovic, P.N. Ross, N.M. Markovic, J. Phys. Chem. B 109 (2005) 14433–14440.
[47] K. Kinoshita, J. Electrochem. Soc. 137 (1990) 845–848.
[48] J.M. Feliu, E. Herrero, V. Climent, Electrocatalytic Properties of Stepped Surfaces, in Catalysis in Electrochemistry: From Fundamentals to Strategies for Fuel Cell Development, John Wiley & Sons, Hoboken, New Jersey, 2011.
[49] K. Kinoshita, Electrochemical Oxygen Technology, the Electrochemical Society Series, John Wiley & Sons, New York, 1992.
[50] S.K. Roy, M.E. Orazem, B. Tribollet, J. Electrochem. Soc. 154 (2007) B1378–B1388.
[51] A. López-Cudero, J. Solla-Gullón, E. Herrero, A. Aldaz, J.M. Feliu, J. Electroanal. Chem. 644 (2010) 117–126.